A Wall-Cooled Fixed-Bed Reactor for Gas-Phase Fischer-Tropsch Synthesis

Arvind. Nanduri[1] and Patrick L. Mills[*1]
[1]Texas A&M University-Kingsville, Department of Chemical & Natural Gas Engineering
*Corresponding author: Texas A&M University-Kingsville, Department of Chemical & Natural Gas Engineering, EC 303D, MSC 193, Kingsville, TX-78363-8202, USA. Email: Patrick.Mills@tamuk.edu

Abstract: A 2-D catalyst pellet model coupled with a non-isothermal 1-D heterogeneous axial dispersion reactor model was numerically simulated to analyze both particle-level and reactor-level performance of three different catalyst particle shapes (sphere, cylinder, and hollow cylinder/ring) for the gas-phase Fischer-Tropsch Synthesis (FTS). A Fe-based micro-kinetic olefin re-adsorption model developed by Wang *et al*. (2008) was coupled with the Soave-Redlich-Kwong (SRK) equation of state to describe the particle-scale transport-kinetic interactions and phase behavior for the gas-phase FTS [3]. The reactor-scale axial temperature and specie concentration profiles, CO conversion, axial diesel range concentration profiles, and reactor-scale methane-based diesel selectivity were analyzed to compare the reactor-scale performance of spherical, cylindrical and hollow cylindrical catalyst particle shapes.

Keywords: Fischer-Tropsch Synthesis, heterogeneous axial dispersion model, extrusion coupling, linear projection, F-T gas phase micro-kinetics.

1. Introduction

Fischer-Tropsch Synthesis (FTS) is a highly exothermic polymerization reaction of syngas ($CO+H_2$) in the presence of Fe/Co/Ru-based catalysts to produce a wide range of paraffins, olefins and oxygenates, which is often called *syncrude*. Multi-Tubular Fixed Bed Reactors (MTFBR) and Slurry Bubble Column reactors (SBCR) are widely employed for FTS processes [1 & 11]. A MTFBR, used for gas-phase F-T synthesis, is similar to a shell and tube heat exchanger with a catalytic reaction taking place on the tube-side. A coolant, generally water, flows on the shell-side to maintain isothermal conditions in the reactor. To model such a system, detailed knowledge about shell-side interactions coupled with tube-side catalytic reaction is required, and modeling a single fixed-bed will provide information on the reactor-scale fluid-solid transport interactions.

A few reactor models for F-T synthesis have been developed in the past to investigate the performance of large-scale commercial reactors [7-10]. However, all the studies were either based on a pseudo-homogeneous reactor model with traditional lumped kinetics or a fixed-bed with only spherical catalyst particles. The use of a pseudo-homogeneous reactor model will not capture the intra-particle diffusional limitations, and for a complex reaction network with liquid products, like F-T synthesis, the intra-particle diffusion limitations severely affect the performance of the reactor. In this study, a 1-D heterogeneous axial dispersion model is used to describe the reactor-scale specie balance in a fixed-bed, and a 1-D energy balance is used to study the axial temperature gradient.

2. Reactor Model

The isothermal 2-D catalyst pellet model and the non-isothermal 1-D heterogeneous axial dispersion reactor model used to describe the catalyst-scale transport-kinetic interactions, and the reactor-scale fluid-solid interactions are presented in this section.

A total number of 20 paraffins (C_1 to C_{20}), 19 olefins (C_2 to C_{20}) and 4 key components (H_2, CO, CO_2, and H_2O) are considered in the reaction network. This leads to 43 nonlinear differential equations for the particle-scale specie mass balances, 43 nonlinear differential equations for the reactor-scale specie mass balances and one reactor-scale energy balance equation. A total of 87 nonlinear coupled ODEs are numerically solved using COMSOL Multiphysics[TM]. The micro-kinetic and thermodynamic expressions used in the model and the algorithm for vapor-liquid equilibria calculations can be found elsewhere [2-4 & 6]. The catalyst particle shapes used in this study are shown in Figure 1.
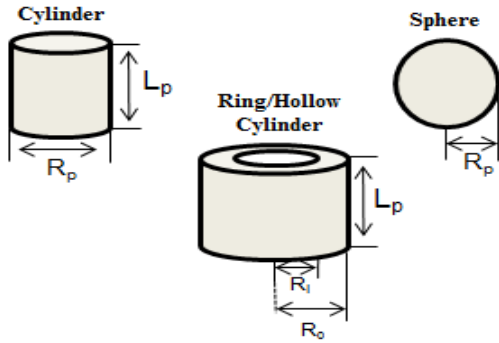
Figure 1. Catalyst particle shapes used in the F-T reactor model.

2.1 Specie mass balance and energy balance equations

The particle-scale specie mass balance equations for various catalyst pellet shapes are summarized below, where $\xi = r/R_p$ for spherical & cylindrical shapes, and $\xi = (r-R_i)/(R_o-R_i)$ & $\delta = R_o-R_i$ for hollow cylinder catalyst shape:

Spherical catalyst pellet:

$$\frac{1}{\xi^2}\frac{\partial}{\partial\xi}\left(D_{ei}\xi^2\frac{\partial C_i}{\partial\xi}\right) = -\rho_p R_p^2 \sum_j \alpha_{ij}R_{ij}$$

Cylindrical catalyst pellet:

$$\frac{1}{\xi}\frac{\partial}{\partial\xi}\left(D_{ei}\xi\frac{\partial C_i}{\partial\xi}\right) = -\rho_p R_p^2 \sum_j^{44}\sum_i^{43} \alpha_{ij}R_{ij}$$

Ring/Hollow cylinder catalyst pellet:

$$\frac{1}{(\xi\delta+R_i)}\frac{\partial}{\partial\xi}\left((\xi\delta+R_i)D_{ei}\frac{\partial C_i}{\partial\xi}\right) = -\rho_p\delta^2\sum_j^{44}\sum_i^{43}\alpha_{ij}R_{ij}$$

The fixed-bed density is calculated from bed porosity as given below.

$$\rho_b = (1-\varepsilon_b)\rho_p$$

The reactor-scale specie mass balance and energy balance equations are summarized below, where $\xi = x/L_r$:

Reactor-scale specie balance:

$$\frac{1}{L_r^2}\frac{d}{d\xi}\left(D_{a,i}\frac{dC_i^{tube}}{d\xi}\right) + \frac{u}{L_r}\frac{dC_i^{tube}}{d\xi}$$

$$= \rho_b\eta_i\sum_j^{44}\sum_i^{43}\alpha_{ij}R_{ij}$$

Reactor-scale energy balance:

$$\frac{\rho_{gas}C_{p,gas}u_s}{L_r}\frac{dT_{tube}}{d\xi} = \frac{U_{overall}4(T_{tube}-T_{cool})}{D_r}$$

$$-\rho_b\sum_i\eta_i\sum_j(-\Delta H_{ij})R_{ij}$$

2.2 Boundary conditions

The boundary conditions for both the catalyst pellet and the fixed-bed correspond to specified values at the pellet surface and reactor inlet (Dirichlet condition), and zero flux at the pellet center and reactor outlet (Neumann condition).

Specie mass balance for spherical and cylindrical catalyst pellet:

At $\xi = 1$ (pellet surface), $C_i = C_i^{tube}$ and $\xi = 0$ (pellet center), $dC_i/d\xi = 0$

Specie mass balance for ring catalyst pellet:

At $\xi = 1$ (pellet outer surface), $C_i = C_i^{tube}$ and $\xi = 0$ (pellet inner surface), $C_i = C_i^{tube}$

Specie mass balance for fixed-bed:

At $\xi = 0$ (entrance), $C_i^{tube} = C_{inlet}$ and $\xi = 1$ (outlet), $dC_i^{tube}/d\xi = 0$

Energy balance for fixed-bed:

At $\xi = 0$ (entrance), $T_{tube} = T_{inlet}$ and $\xi = 1$ (outlet), $dT_{tube}/d\xi = 0$

3. Use of COMSOL Multiphysics

The critical aspect of reactor modeling in COMSOL Multiphysics[TM] is the coupling between the catalyst-scale transport-kinetic interactions and the reactor-scale fluid-solid interactions through the *transport of diluted species* module. This can be achieved by using *extrusion coupling* and *linear projection*. The

coupling strategy is illustrated in Figure 2. The particle domain is defined by a 2-D geometry, and the reactor domain is defined by a 1-D geometry. To obtain the observed rate on the reactor-scale, the overall effectiveness factor is calculated from the integral rate at each grid point on the boundary that is coupled to the reactor geometry. To calculate the integral rate at every grid point on the coupled boundary, *linear projection* in COMSOL Multiphysics^{TM} is used. The effectiveness factor for each component is estimated, which is then used to calculate the observed rate on the reactor geometry. The temperature from the 1-D reactor-scale energy balance is also coupled on to the 2-D particle domain. The 2-D particle domain was meshed using triangular elements, and the coupled boundaries were meshed with equal number of elements.
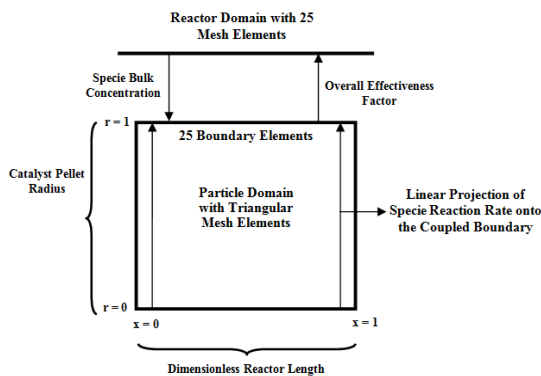
Figure 2. The extrusion coupling and linear projection strategy for a 1-D heterogeneous Fischer-Tropsch reactor model.

The 2-D particle domain is first simulated without coupling to the reactor domain to get an initial solution, which is then used as an initial guess for quick and error free convergence. Once the particle domain converges, the coupling variables are activated with a small reactor length (about 0.1 m), and then the length is slowly increased to achieve smooth convergence. The 1-D energy equation is solved using the *coefficient form PDE solver* module. The energy balance equation encounters severe numerical instabilities due to the high exothermic nature of the reaction. To avoid convergence issues, the net heat of the reaction is multiplied with a perturbation factor of 10^{-10}, and then this factor is slowly increased to 1.

The numerical instabilities and the use of inbuilt logical operators to avoid negative specie concentrations are discussed elsewhere [6]. Mesh refinement was manually performed until the concentration profiles were relatively constant and satisfied the convergence criterion. The catalyst properties and operating conditions are listed in Table 1 – 2.

Table 1. Catalyst properties [2, 6]

Pellet Density, ρ_p	1.95 x 10^6 (gm/m^3)
Porosity of pellet, ε	0.51
Tortuosity, τ	2.6
Catalyst dimensions	
Spherical pellet	R_p = 1.5 mm
cylindrical pellet	L_p = 3 mm & R_p = 1 mm
hollow cylindrical pellet	L_p = 3 mm, R_o = 2 mm & R_i = 1 mm

**Table 2**. Reactor operating conditions [9].

L_r	12 m
D_r	5 cm
T_{inlet}	493 ^{o}K
P_{inlet}	25 bar & 30 bar
H_2/CO	2
u_s	0.55 m/s
T_{cool}	493 ^{o}K
$U_{overall}$	364 W/m^{2}K
ν_{gas}	$4*10^{-6}$ (m^2/s)
ε_b	Sphere: 0.58[9] Cylinder: 0.36[12] Ring: 0.48[12]

4. Results

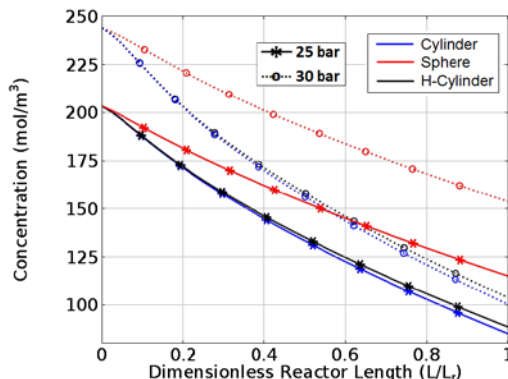### 4.1 Axial and particle-scale concentration profiles of key reactants

The reactor-scale axial concentration profiles of the key components (H$_2$, CO, CO$_2$ and H$_2$O)

under typical FTS operating conditions for different catalyst particle shapes are shown in Figure 3 - 6.
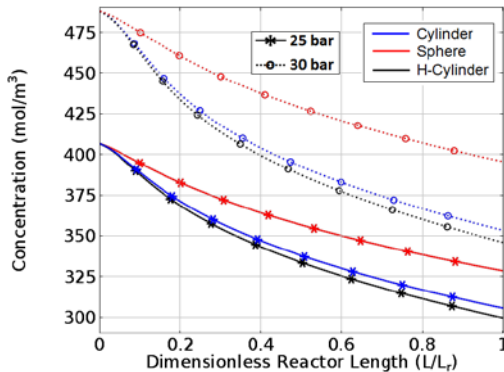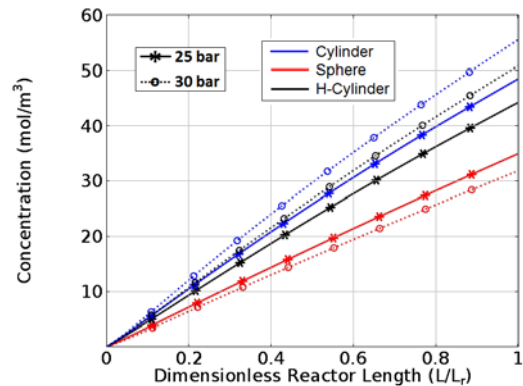

Figure 3. Axial concentration profiles of H_2 in the fixed-bed (reactor length L_r = 12 m, reactor diameter D_r = 5 cm, T = 493 K, P = 25 bar & 30 bar, and H_2/CO = 2).

The concentration profiles of all the key reactants follow similar trend for both cylinder and ring catalyst particle shapes. The profiles exhibit a rapid decreasing behavior, in the case of H_2, and CO, and a rapid increasing behavior, in the case of H_2O, at the reactor entrance for both the cylinder and ring catalyst particle shapes. This behavior of the profiles is due to the occurrence of hot spots at the reactor entrance. The CO concentration profiles show that the cylinder, and the ring catalyst particle shapes predict higher conversion of CO on a reactor-scale, when compared to the spherical catalyst shape.
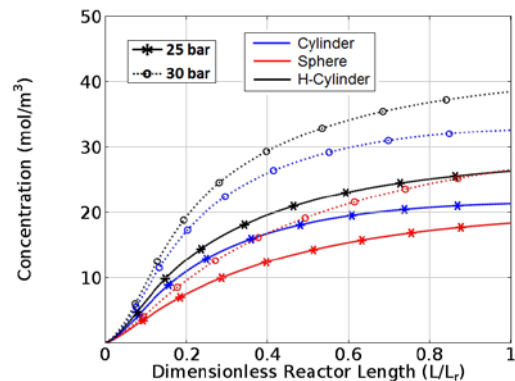

Figure 4. Axial concentration profiles of CO in the fixed-bed (reactor length L_r = 12 m, reactor diameter D_r = 5 cm, T = 493 K, P = 25 bar & 30 bar, and H_2/CO = 2).

It is important to study the intra-particle concentration profiles of CO_2 on a reactor-scale, as the Water-Gas-Shift (WGS) reaction controls the availability of CO for the F-T synthesis. To study the CO_2 profiles on a reactor-scale, the volume averaged intra-particle CO_2 concentration is calculated on every grid point on the coupled boundary using the linear projection scheme as discussed in Section 3.
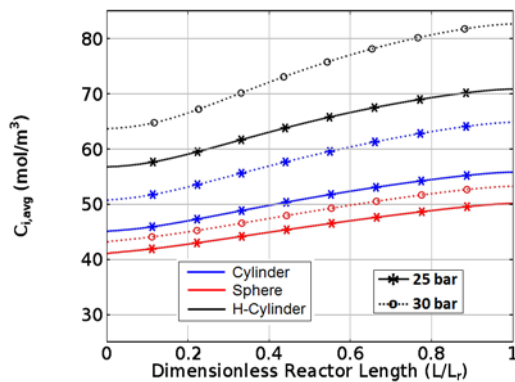

Figure 5. Axial concentration profiles of CO_2 in the fixed-bed (reactor length L_r = 12 m, reactor diameter D_r = 5 cm, T = 493 K, P = 25 bar & 30 bar, and H_2/CO = 2).

Figure 6. Axial concentration profiles of H_2O in the fixed-bed (reactor length L_r = 12 m, reactor diameter D_r = 5 cm, T = 493 K, P = 25 bar & 30 bar, and H_2/CO = 2).

The average intra-particle CO_2 concentration profiles for different catalyst particle shapes are shown in Figure 7. It can be noted that the average CO_2 concentration increases not only along the length of the fixed-bed, but also with the increase in operating pressure. It can also be noted that the magnitude of difference between the average CO_2 concentration for the spherical

catalyst, for 25 and 30 bar, is less when compared to the other particle shapes. This can be explained by noting that the reverse WGS reaction rate becomes limited in spherical catalyst with increase in pressure [10]. Whereas, the magnitude of difference between the average CO_2 concentration for cylinder and ring catalyst shapes increases with increase in operating pressure, along the fixed-bed. This shows that the WGS reaction is not limited in these shapes, as it is the case with the spherical catalyst shape. These results provide an important baseline to understand the F-T reaction chemistry in a fixed-bed with non-spherical catalyst particle shapes.

Figure 7. Average concentration of CO2 in the catalyst pellet along the length of the fixed-bed (reactor length L_r = 12 m, reactor diameter D_r = 5 cm, T = 493 K, P = 25 bar & 30 bar, and H_2/CO = 2).

4.2 Axial temperature profiles

The axial temperature profiles of the fixed-bed for different catalyst particle shapes are shown in Figure 8. The temperature profiles show that the cylinder and ring catalyst particle shapes predict hot spots of similar magnitude, but higher than that corresponding to the spherical catalyst shape. The magnitudes of hot spots are listed in Table 3. The profiles show that the hot spot occurs at the reactor inlet, and the magnitude increases with an increase in operating pressure. As mentioned in section 4.1, this particular behavior of the axial temperature increases the F-T reaction rate, resulting in rapid consumption of the reactants in the F-T reaction network. It has been mentioned in the literature that by using a recycle stream, the hot spots will be pushed further along the reactor making it thermally more stable [9, 10].
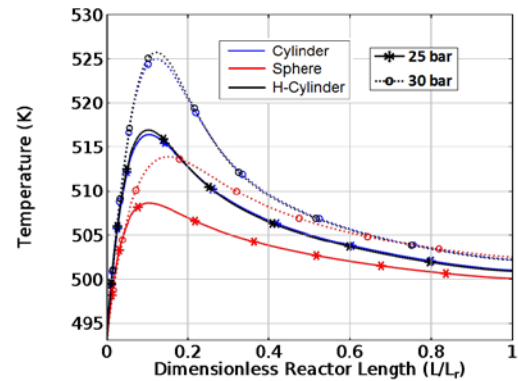
Figure 8. Axial Temperature profiles in the fixed-bed (reactor length L_r = 12 m, reactor diameter D_r = 5 cm, T = 493 K, P = 25 bar & 30 bar, and H_2/CO = 2).

**Table 3**. Hot spot temperature magnitudes for different catalyst particle shapes.

Shape	T_{max}	
	25 bar	**30 bar**
Cylinder	516 K	525 K
H-Cylinder	517 K	526 K
Sphere	509 K	513 K

A high temperature in the reactor facilitates the methanation reaction and also breaks down diesel range hydrocarbons to small chain paraffins. Hence, it is crucial to study the axial temperature profiles of the fixed-bed, as it dictates the F-T product selectivity.

4.3 Reactor-scale CO conversion profiles

The reactor-scale CO conversion profiles for different catalyst particle shapes are shown in Figure 9. The cylinder and ring catalyst shapes predict a higher conversion of CO when compared to the spherical catalyst shape. This can be explained by noting that the temperature of the fixed-bed is higher at the inlet, as explained in Section 4.2, resulting in the rapid participation of CO in the F-T reaction network. Interestingly, the CO conversion reduces with increasing in pressure for spherical catalyst shape when compared to the cylinder and ring catalyst shapes. As mentioned in Section 4.1, this can be explained by noting that the reverse WGS reaction rate becomes limited with an increase in

pressure (30 bar) resulting in relatively less CO concentration in the bulk phase when compared to the low operating pressure conditions (25 bar). The CO conversion values alone do not suggest the superiority of the cylinder and ring catalyst particle shapes over the spherical catalyst shape, as it is important to study the diesel range hydrocarbon selectivity over short chain paraffins like methane.
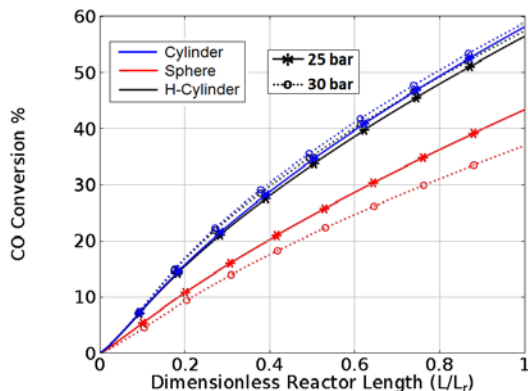
Figure 9. CO conversion in the fixed-bed (reactor length L_r = 12 m, reactor diameter D_r = 5 cm, T = 493 K, P = 25 bar & 30 bar, and H_2/CO = 2).
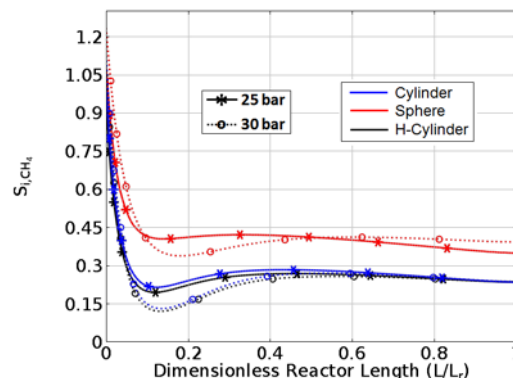
4.4 Reactor-scale methane-based diesel selectivity and concentration profiles of diesel range

The reactor-scale diesel range concentration profiles and methane-based diesel selectivity ($S_{i,CH4}$) for all the catalyst particle shapes are shown in Figures 10 - 11.
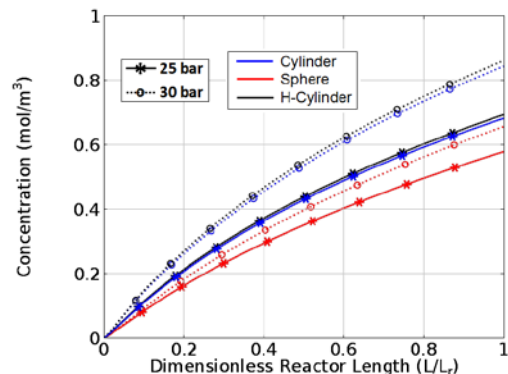
Figure 10. Axial concentration profiles of diesel in the fixed-bed (reactor length L_r = 12 m, reactor diameter D_r = 5 cm, T = 493 K, P = 25 bar & 30 bar, and H_2/CO = 2).

It can be noted from the axial diesel concentration profiles that the cylinder and ring catalyst particle shapes predict a higher concentration of diesel range hydrocarbons than the spherical catalyst shape. The diesel range concentration increases with an increase in operating pressure for all the catalyst particle shapes.

Figure 11. Reactor-scale methane-based diesel selectivity (reactor length L_r = 12 m, reactor diameter D_r = 5 cm, T = 493 K, P = 25 bar & 30 bar, and H_2/CO = 2).

The methane-based diesel selectivity profiles follow a decreasing trend at the reactor inlet due to the occurrence of hot spots, which results in the formation methane and other short chain paraffins. It is only after the hot spot region that the diesel selectivity gradually increases along the fixed-bed. It can also be noted that the spherical catalyst is more selective towards the diesel range than the other two shapes. This is due to the large magnitude of hot spots for cylinder and ring particle shapes, as mentioned in Section 4.4, resulting in high concentration of methane at the inlet of the reactor for these shapes. However, the diesel range concentration profiles suggest that cylinder and ring particle shapes are preferred over the spherical catalyst shape.

5. Conclusions

A 2-D catalyst pellet model coupled with a 1-D heterogeneous axial dispersion reactor model using sphere, cylinder and ring catalyst particle shapes was successfully analyzed for the first time using COMSOL Multiphysics. Micro kinetic rate equations, when coupled with

intraparticle transport effects and vapor-liquid equilibrium phenomena, captures the transport-kinetic interactions and phase behavior for gas-phase FT catalysts on both the particle-scale and reactor-scale. This work demonstrates that COMSOL can be a powerful numerical engine in solving highly coupled reactor model, with different catalyst particle shapes, by utilizing the in-built *extrusion coupling* and *linear projection* schemes. The CO conversion, and the reactor-scale diesel range concentration profiles results suggest that cylinder and hollow ring shapes are preferred over spherical particle shapes, but the magnitude of the hot spot is greater for those shapes. This may lead to a higher rate of catalyst deactivation, reduce the catalyst mechanical strength and generate unsafe reactor operating conditions. The results in the current work show the importance of understanding the axial temperature profile of a single fixed-bed in order to efficiently design a MTFBR.

6. Nomenclature

C_i	Concentration of species 'i' in the catalyst pellet (mol/m^3)
$C_{i,avg}$	Intra-particle average concentration $\frac{\int C_i dv}{V_p}$ (mol/m^3)
C_i^{tube}	Concentration of species 'i' in the fixed bed (mol/m^3)
$C_{p,gas}$	Heat capacity of feed gas (J/mole K)
$D_{a,i}$	Axial dispersion coefficient ($u^{int}*D_p/Pe_i$) (m^2/s)
D_{ei}	Effective diffusivity of species 'i' (m^2/s)
$D_{i,B}$	Bulk diffusivity of component i (m^2/s)
D_p	Pellet diameter ($2*R_p$) (mm)
D_r	Reactor diameter (cm)
L	Number of moles in the liquid phase (moles)
L_r	Reactor length (m)
P	Pressure (bar)
Pe_i	Peclet number of component i
r	Radial coordinate (mm)
R_p	Radius of catalyst pellet (mm)
R_{ij}	Rate of component i in jth reaction (mol kg^{-1} s^{-1})
Re	Reynolds number ($D_p*u_s* \rho_{gas}/ \mu_{gas}$)
$S_{i,CH4}$	Methane-based diesel selectivity $\left(\frac{\Sigma_{i,j} \alpha_{ij} R_{ij}}{\Sigma_{CH_4,j} \alpha_{CH_4,j} R_{CH_4,j}} \right)$
Sc_i	Schmidt number ($\mu_{gas}/ \rho_{gas}*D_{i,B}$)
T	Temperature (K)
T_{cool}	Coolant temperature (K)
T_{max}	Hot spot temperature (K)
T_{tube}	Reactor axial temperature (K)

u^{int}	Interstitial velocity (u_s/ ε_b) (m/s)
$U_{overall}$	Overall heat transfer coefficient (W m^{-2} K^{-1})
u_s	Reactor superficial velocity (m/s)
V	Number of moles in vapor phase
x	Axial coordinate (mm)

Greek Letters

α_g	Intra-particle vapor fraction
α_{ij}	Stoichiometric coefficient of component i in reaction j
δ	Hollow cylinder thickness (mm)
ε_p	Catalyst pellet porosity
ε_b	Bed porosity
η_i	effectiveness factor of component i $\left(\frac{\int \Sigma_{ij} \alpha_{ij} R_{ij}^{pellet} dv}{\left(\Sigma_{ij} \alpha_{ij} R_{ij}^{pellet} V_p \right)_{surface}} \right)$
μ_{gas}	Feed gas viscosity ($\nu_{gas}*\rho_{gas}$) (kg m^{-1} s^{-1})
ν_{gas}	Kinematic viscosity of feed gas (m^2/s)
ξ	dimensionless spatial coordinate
ρ_b	Bed density (kg/m^3)
ρ_{gas}	Feed gas density (kg/m^3)
ρ_p	Density of catalyst pellet (kg/m^3)
τ	Catalyst tortuosity

7. References

1. D. A. Wood, C. Nwaoha, and B. F. Towler, *Journal of Natural Gas Science and Engineering*, **9**, 196-208 (2012)
2. Yi-Ning Wang, Yuan-Yuan Xu, Hong-Wei Xiang, Yong-Wang Li, and Bi-Jiang Zhang, *Industrial & Engineering Chemistry Research*, **40**, 4324-4335 (2001)
3. Y. N. Wang, Y. W. Li, L. Bai, Y. L. Zhao, and B. J. Zhang, *Fuel*, **78**, 911-917 (1999)
4. Yi-Ning Wang, Wen-Ping Ma, Yi-Jun Lu, Jun Yang, Yuan-Yuan Xu, Hong-Wei Xiang, Yong-Wang Li, Yu-Long Zhao, Bi-Jiang Zhang, *Fuel*, **82**, 195-213 (2003)
5. Yong Yang, Hong-Wei Xiang, Yuan-Yuan Xu, Liang Bai, Yong-Wang Li, *Applied Catalysis A: General*, **266**, 181-194 (2004)
6. Arvind Nanduri, and Patrick L. Mills, *Proceedings of the 2014 COMSOL Conference in Boston* (2014)
7. G. Bub, and M. Baerns, *Chemical Engineering Science*, **35**, 348-355 (1980)
8. H. E. Atwood, and C. O. Bennett, *Industrial & Engineering Chemistry Process Design and Development,* **18**, 163-170 (1979)
9. A. Jess, and C. Kern, *Chemical Engineering Technology,* **35**, 369-378 (2012)
10. Y. N. Wang, Y. Y. Xu, Y. W. Li, Y. L. Zhao, and B. J. Zhang, *Chemical Engineering Science,* **58**, 867-875 (2003)
11. B. H. Davis, *Topics in Catalysis,* **32**, 143-168 (2005)
12. Damjan Nemec, and Janez Levec, *Chemical Engineering Science*, **60**, 6947-6957 (2005)